ACS OMEGA

Open Access

http://pubs.acs.org/journal/acsodf

Article

Improving the Performance of Si/PEDOT:PSS Hybrid Solar Cells with More Economical and Environmentally Friendly Alcohol Ether Solvents

Guijun Zhang, Hua Peng, Qianwen Wei, Zheng Zhou, Haixia Wu, Jingjing Luo, Juan Wang,* Xiaoming Wen,* and Yu Yang*

Cite This: *ACS Omega* 2024, 9, 15040−15051

Read Online

ACCESS | Metrics & More | Article Recommendations | Supporting Information

ABSTRACT: The photoelectric characteristics of poly(3,4-ethylenedioxythiophene):polystyrene sulfonate (PEDOT:PSS) films significantly affect the power conversion efficiency and stability of Si/PEDOT:PSS hybrid solar cells. In this paper, we investigated PEDOT:PSS modification with alcohol ether solvents (dipropylene glycol methyl ether (DPM) and propylene glycol phenyl ether (PPH)). The reduction of PSS content and the transformation of the PEDOT chain from benzene to a quinone structure in PEDOT:PSS induced by doping with DPM or PPH are the reasons for the improved conductivity of PEDOT:PSS films. DPM and PPH doping improves the quality of silicon with the PEDOT:PSS heterojunction and silicon surface passivation, thereby reducing the surface recombination of charge carriers, which improves the photovoltaic performance of Si/PEDOT:PSS solar cells. Comparing the power conversion performance (PCE) and air stability of Si/PEDOT:PSS solar cells with DPM (13.24%), DPH (13.51%), ethylene glycol (EG, 13.07%), and dimethyl sulfoxide (DMSO, 12.62%), it is suggested that doping with DPM and DPH can replace DMSO and EG to enhance the performance of Si/PEDOT:PSS solar cells. The EG and DMSO solvents not only have a certain toxicity to the human body but also are not environmentally friendly. In comparison to DMSO and EG, DPM and DPH are more economical and environmentally friendly, helping to reduce the manufacturing cost of Si/PEDOT:PSS solar cells and making them more conducive to their commercial applications.

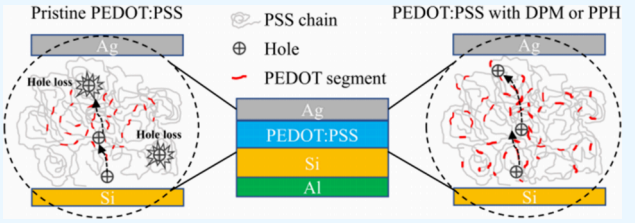

1. INTRODUCTION

The silicon-based hybrid solar cell is a novel variation derived from traditional monocrystalline silicon-based solar cells. In contrast to traditional crystalline silicon solar cells, the silicon-based hybrid solar cell eliminates high-temperature junction making and doping processes. It is characterized by a simple preparation process, low cost, and potential mechanical flexibility.[1] This is due to the presence of the organic conductive polymer material poly(3,4-ethylenedioxythiophene):polystyrene sulfonate. Therefore, in numerous studies on silicon-organic/inorganic hybrid solar cells, the Si/PEDOT:PSS structure has emerged as the most researched among silicon-based hybrid solar cells (HSCs). This is attributed to its favorable characteristics, including good electrical conductivity, light transmission, a straightforward processing method, and adjustable color.[2−9] Various approaches have been recently developed to enhance the efficiency of Si/PEDOT:PSS HSCs by modifying the silicon surface structure, leading to a maximum power conversion efficiency (PCE) exceeding 17%.[10,11] However, processing the silicon surface results in higher manufacturing costs.

One of the key factors affecting the performance of Si/PEDOT:PSS solar cells is the photoelectric characteristics of the PEDOT:PSS film, as it plays a crucial role in the process of forming PEDOT:PSS/Si heterojunctions and facilitating charge transport with Si.[12,13] In general, if the original PEDOT:PSS is not doped, then the conductivity of the dried film will be very poor, generally less than 1 S/cm (PH1000). To improve their conductivity, researchers doped by adding polar, nonpolar, or ionic cosolvents.[3,5,14−16] For example, Srivastava et al. recently reported enhancing the solar cell and photoelectric performance of PEDOT:PSS using methanol and 2-propanol alcohol-based solvents.[3] Among the doping modifications of PEDOT:PSS, ethylene glycol (EG) and dimethyl sulfoxide (DMSO) are the most studied.[17−23] For instance, Yu et al. used 0.2 wt % Triton X-100 doping in the 5 wt % DMSO-doped PEDOT:PSS solution, and the device exhibited the best performance, achieving a PCE of

Received: November 17, 2023
Revised: February 15, 2024
Accepted: February 23, 2024
Published: March 19, 2024

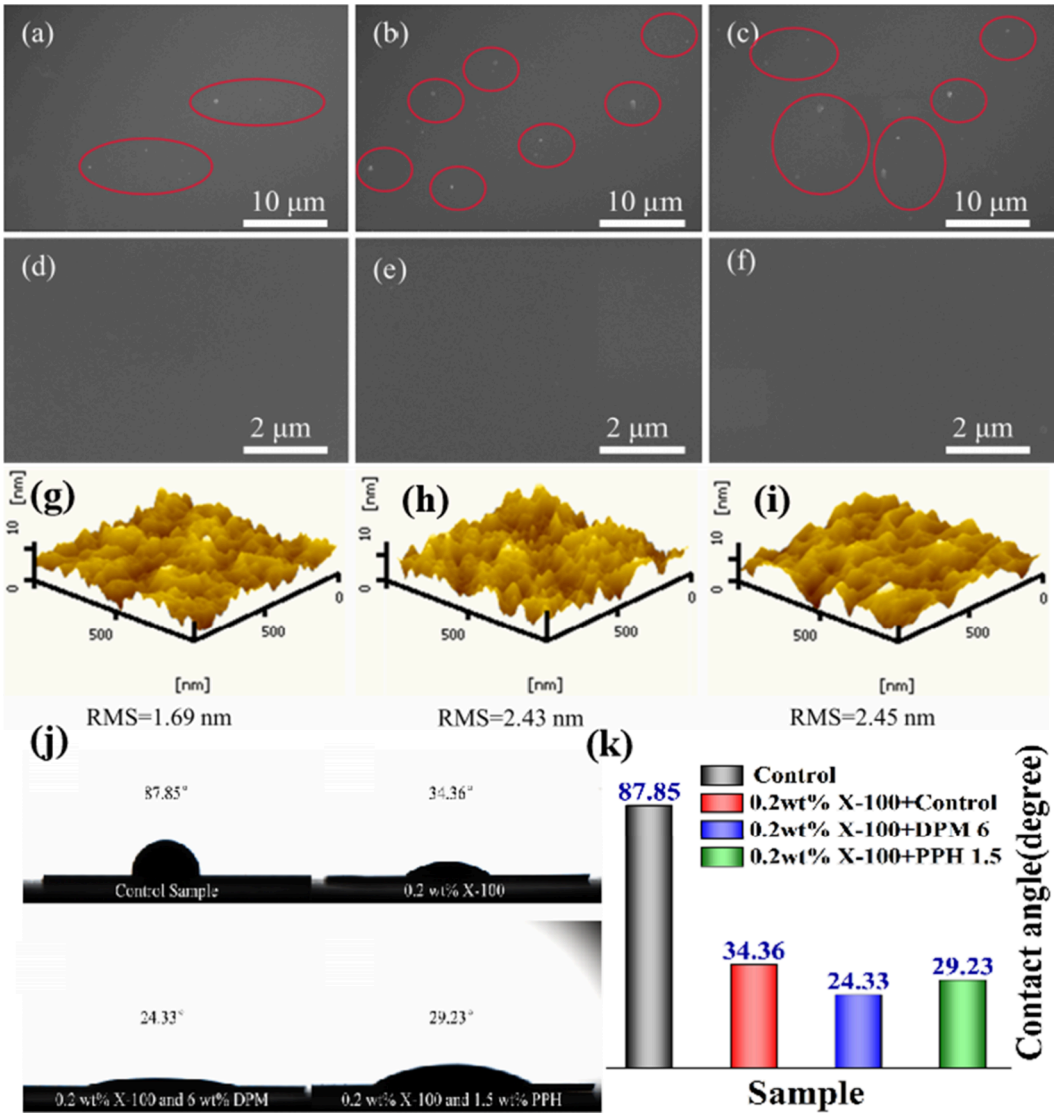

Figure 1. SEM images of PEDOT:PSS films: (a, d) original, (b, e) doped with 6 wt % DPM, and (c, f) doped with 1.5 wt % PPH. AFM diagram of the films: (g) original and (h) doped DPM or (i) PPH. (j) Contact angle images of different PEDOT:PSS films. (k) Contact angle comparison of different PEDOT:PSS films (control, control + X-100, X-100 + DPM, and X-100 + PPH).

13.12%.[18] Thomas and Leung reported that the hybrid solar cell made on a planar Si substrate using the mixed cosolvent of EG and methanol (MeOH)-engineered PEDOT:PSS film shows a high efficiency exceeding 14.6%.[23] Due to the high dielectric constant and high boiling point of PEDOT:PSS, the insulating PSS can be removed by weakening the interaction between PEDOT and PSS.[24−27] However, ethylene glycol (EG)[28−30] and dimethyl sulfoxide (DMSO)[31,32] have certain negative effects on human beings and the environment.

Alcohol ether solvents, such as dipropylene glycol methyl ether (DPM)[33] and propylene glycol phenyl ether (PPH),[34] are widely used in the field of environmentally friendly water-based coatings. DPM is a colorless, transparent liquid with a faint ether taste. It possesses characteristics such as low toxicity, low viscosity, low surface tension, good solubility, and coupling ability, making it a preferred solvent for coatings and dyes. PPH finds extensive use in automotive and automotive repair coatings due to its nontoxic nature, good miscibility, excellent bonding and coupling ability, and low surface tension. Compared with DMSO and EG, DPM and PPH are more environmentally friendly and cost-effective, contributing to the commercialization of Si/PEDOT:PSS solar cells. However, there has been limited research on the doping modification of PEDOT:PSS by DPM or PPH. Therefore, studying the doping modification of the organic layer PEDOT:PSS by DPM and PPH holds a certain reference value and significance.

In this paper, we investigated the effects of DPM and PPH doping on the microscopic morphology and photoelectric properties of PEDOT:PSS films as well as the optimal concentration of DPM and PPH-doped PEDOT:PSS films. The reduction of the PSS content and the transformation of the PEDOT chain from benzene to a quinone structure in PEDOT:PSS induced by DPM or PPH doping are the reasons for the improved conductivity of PEDOT:PSS films. Doping with DPM and PPH not only increased the conductivity of the original film (0.015 S/cm) to 746.27 S/cm (DPM) and 710.21 S/cm (PPH) but also improved the PCE of Si/PEDOT:PSS solar cells from 0.74% to 13.24% (DPM) and 13.51% (PPH) for the original solar cells. Modified PEDOT:PSS with DPM and PPH can enhance junction formation and surface

https://doi.org/10.1021/acsomega.3c09187
ACS Omega 2024, 9, 15040−15051

passivation (reducing the surface recombination of charge carriers) on the silicon surface. Additionally, we compared the PCE of Si/PEDOT:PSS solar cells doped with DPM (13.24%), PPH (13.51%), ethylene glycol (EG, 13.07%), and dimethyl sulfoxide (DMSO, 12.62%). We concluded that the use of DPM and PPH doping can replace the solvents DMSO and EG, which are often used for doping modified PEDOT:PSS. Compared with DMSO and EG, DPM and PPH are more economical and environmentally friendly, helping to reduce the manufacturing cost of Si/PEDOT:PSS solar cells and making them more conducive to commercial applications.

2. RESULTS AND DISCUSSION

2.1. The Effect of DPM and PPH Doping on the Microscopic Morphology of PEDOT:PSS Films. In the Supporting Information, Figure S1a illustrates the structure and working principle of typical Si/PEDOT:PSS HSCs. The chemical structures of PEDOT:PSS, DPM, and PPH are depicted in Figure S1b. The PEDOT:PSS film was prepared by spin coating. To investigate the influence of microstructure resulting from the doping of PEDOT:PSS films with different solvents, we conducted a series of observations using scanning electron microscopy (SEM), atomic force microscopy (AFM), and a contact angle tester. PEDOT:PSS films doped with various solvents were obtained through the spin coating method (the preparation process is detailed in Figure S1c). We explored the impact of different solvent doping on the microstructure of PEDOT:PSS films through observations conducted with scanning electron microscopy (SEM), atomic force microscopy (AFM), and a contact angle tester. The PEDOT:PSS films doped with different solvents were prepared using the spin coating method. (The preparation process is shown in Figure S1c.)

Figure 1a−f displays SEM images of the original PEDOT:PSS films and DPM- or PPH-doped PEDOT:PSS films. It is evident that the film contains free PSS (depicted as white dots) and PEDOT:PSS complexes. The original film (Figure 1a) exhibits relatively less PSS on the surface, while doping with 6 wt % DPM (Figure 1b) and 1.5 wt % PPH (Figure 1c) results in more PSS. The separation of the two components is attributed to the solubility difference in the system of two polymer additives and the differences in evaporation rates between water and the additive-driven process.[35] High-boiling-point solvents such as DPM and PPH serve as effective solvents for PSS. During the drying process after spin coating, water evaporates rapidly, leading to solid−liquid separation. In this process, the PEDOT:PSS complex precipitates first, and free PSS is concentrated into the remaining solution rich in additives. Continued drying ensures that DPM or PPH solvents maintain the phase separation of PEDOT from PSS on a smaller nanometer scale. Consequently, the incorporation of DPM or PPH significantly enhances the separation of PEDOT and PSS in the PEDOT:PSS film. After spin coating, the PSS component is expelled and floats on the surface of the film. Figures 1d−f demonstrates that the spin-coated PEDOT:PSS film is uniform and smooth as a whole. This uniformity is crucial in reducing defects that can adversely affect film quality and the performance of PEDOT:PSS/Si solar cell devices.

In addition, the morphological characteristics of the PEDOT:PSS films were analyzed by atomic force microscopy (AFM). The original PEDOT:PSS film exhibits a fairly smooth and homogeneous surface with a root-mean-square roughness (RMS) of 1.69 nm (Figure 1g). After doping with DPM or PPH, the domain size increases and the film becomes coarser, resulting in an increased RMS to 2.43 and 2.45 nm, respectively. It is worth noting that the PPH-doped film (Figure 1i) is slightly rougher than the DPM-doped film (Figure 1h), possibly due to the steric hindrance of PPH containing a benzene ring structure. In Figure S2, the bright region corresponds to the hydrophobic conducting PEDOT core, while the darker region (lower height) corresponds to the hydrophilic insulating PSS.[36,37] After doping, PEDOT:PSS films show a better-connected PEDOT area, confirming the phase separation between PEDOT and PSS. Therefore, the addition of DPM or PPH induces nanoscale phase separation characterized by the expansion of PEDOT domains and enhanced interconnection between PEDOT phases, resulting in an efficient hole transport pathway. Most of the charge transport in PEDOT:PSS films is largely influenced by the charge transport within the PEDOT chain, which is usually faster.[38] The conjugated structure of PEDOT serves two roles: (1) it can extend the ordered structure region of PEDOT due to the $\pi-\pi$ interaction between loops, and (2) the conjugated structure makes the charge transfer between PEDOT chains easier.[39] Therefore, this structural arrangement explains why the conductivity of the PEDOT:PSS film increases sharply after doping with DPM or PPH.

To investigate the influence of the microstructure of PEDOT:PSS films on the doping with DPM and PPH, we conducted contact angle (CA) tests. As shown in Figure 1j, the original PEDOT:PSS dispersion is challenging to wet and attach to the Si substrate with relatively low surface tension due to the large surface tension, resulting in a contact angle (CA) between the two of 87.85°. Consequently, such dispersions cannot be spin-coated on silicon wafers without the addition of surfactants. After the addition of Triton X-100, the contact angle decreased to 34.36° and PEDOT:PSS was easily spin-coated on the Si sheet. Following the addition of 6 wt % DPM and 1.5 wt % PPH, the contact angle continued to decrease to 24.33° and 29.23°, respectively. This indicates that the addition of the two solvents also reduces the surface tension of the dispersed liquid system and improves the wettability of PEDOT:PSS with respect to Si. This improvement helps in forming a uniform and flat film after drying, reducing electron−hole recombination and facilitating the separation and transmission of charge carriers.[40] The comparison of the contact angle test results can be seen in Figure 1k, where the contact angle was significantly reduced after doping with DPM and PPH.

2.2. The Effect of DPM and PPH Doping on the Photoelectric Properties of the PEDOT:PSS Film and the Change of the PEDOT:PSS Structure. To explore how the photoelectric properties of the PEDOT:PSS film change before and after doping with DPM and PPH, we spin-coated PEDOT:PSS predispersion liquid onto a 1.1 × 1.1 cm^2 quartz glass substrate. After annealing and drying, the substrate was cooled to room temperature and a Ag electrode was deposited. The conductivity (ρ) and charge carrier (hole) concentration (n) of the PEDOT:PSS film were measured by using the Hall test system and the four-probe method. The test results are presented in Table S1. Here, M represents DPM, H represents PPH, and the number after the letter represents the mass percentage of PEDOT:PSS (for example, M2 represents DPM added to 2 wt %). Before doping, the conductivity and carrier concentration of the original PEDOT:PSS film were very low,

https://doi.org/10.1021/acsomega.3c09187
ACS Omega 2024, 9, 15040−15051

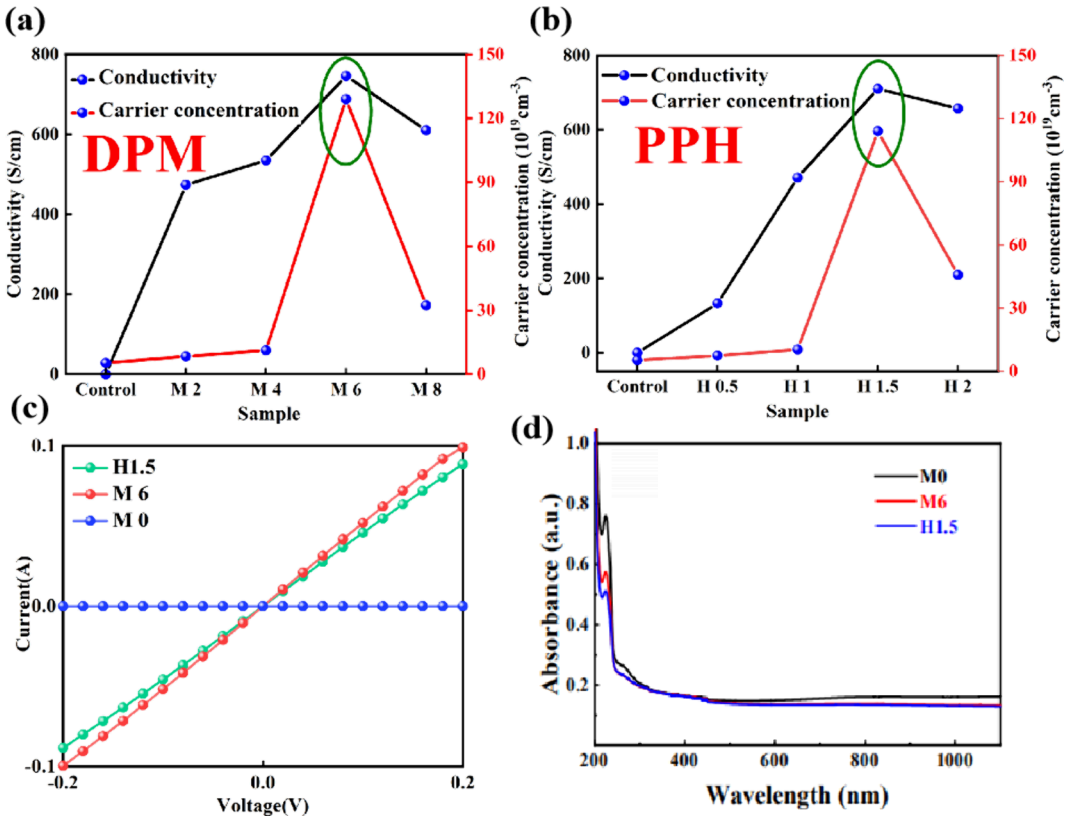

Figure 2. Conductivity and carrier concentration of (a) DPM-doped and (b) PPH-doped PEDOT:PSS films. (c) *I*−*V* curves of DPM 6 and PPH 1.5 were measured under dark conditions. (d) Absorbance of the full wavelengths of the original PEDOT:PSS films doped with DPM and PPH.

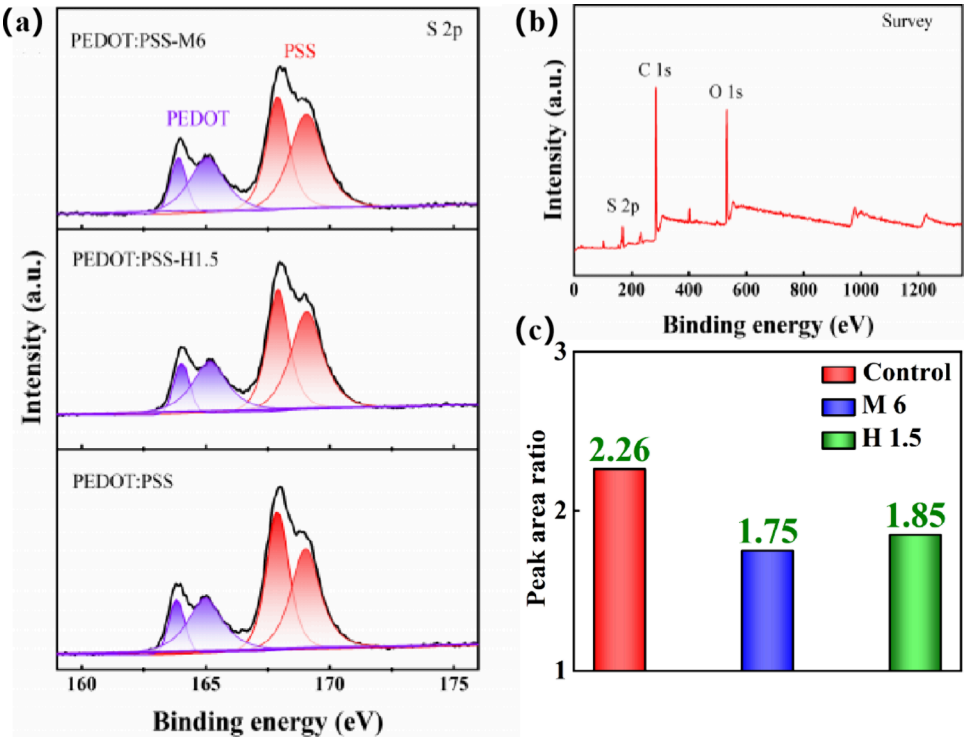

Figure 3. XPS test results: (a) S 2p and (b) survey of XPS; (c) peak area ratio of PSS to PEDOT for the PEDOT:PSS films: original and doped with 6 wt % DPM and 1.5 wt % PPH.

at 0.015 S/cm and 5.29 × 10^{19} cm^{-3}, respectively. This is attributed to the large amount of insulating PSS in the film, leading to poor overall conductivity.

In Figure 2a,b, we can gain a more intuitive understanding of the relationship among conductivity, carrier concentration, and the concentration of DPM or PPH doping. After adding 2 wt

https://doi.org/10.1021/acsomega.3c09187
ACS Omega 2024, 9, 15040−15051

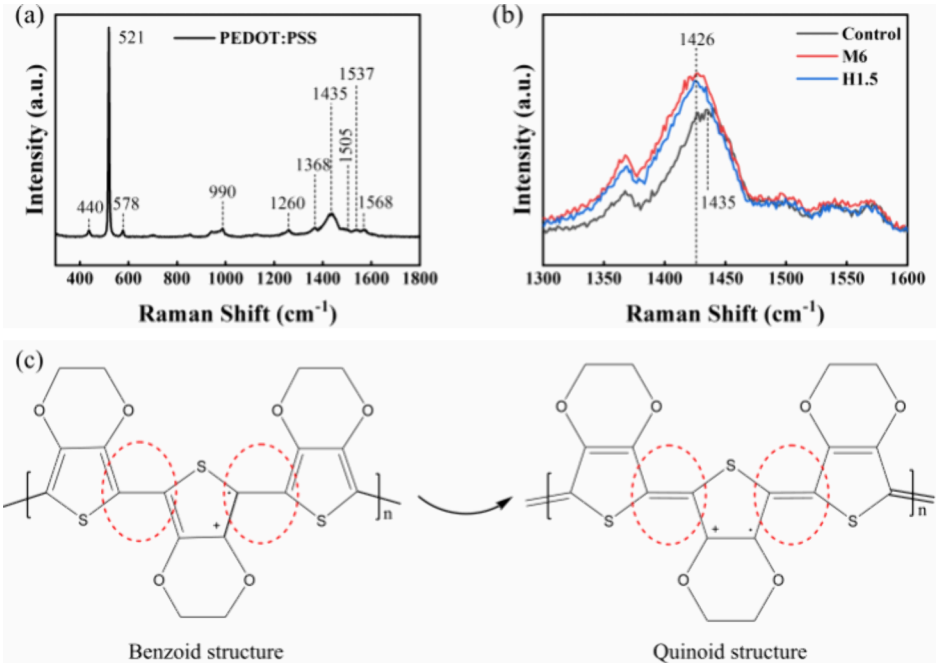

Figure 4. (a) Raman diagram of original PEDOT:PSS films; (b) partial Raman diagram of films: original and doped with 6 wt % DPM or 1.5 wt % PPH; (c) transition of PEDOT from a benzoid structure to a quinoid structure.

% to 8 wt % DPM or 0.5 wt % to 2 wt % PPH, the conductivity and carrier concentration of PEDOT:PSS films improved to varying degrees. When 6 wt % DPM was added, the conductivity and carrier concentration of the film reached peak values of 746.27 S/cm and 1.29 × 10^{21} cm^{-3}, respectively.

Compared with the control sample (M0) without DPM, the film's conductivity and carrier concentration increased nearly 50,000 times and 24 times, respectively. However, with continued DPM doping, the conductivity decreased to 609.76 S/cm, and the carrier concentration also decreased by about an order of magnitude to 3.23 × 10^{20} cm^{-3}. This indicates that more DPM doping does not necessarily yield better results, and excessive solvent can damage the film's integrity. The same trend is observed for PPH doping. When the addition amount is 1.5 wt %, the conductivity and carrier concentration reach peak values of 710.21 S/cm and 1.14 × 10^{21} cm^{-3}, respectively, and start to decrease significantly with further addition. Therefore, we can conclude that the doping with DPM or PPH increases the carrier concentration of the PEDOT:PSS film, improves the film's conductivity, and enhances its overall performance. Additionally, the influence of doping on the electrical conductivity was investigated, as shown in Figure 2c. Higher electrical conductivity was observed in DPM, consistent with the Hall test results.

Through UV−vis absorption spectra, light absorption of the PEDOT:PSS film was detected, as shown in Figure 2d. It has been reported that the strong peaks at low wavelengths (below 300 nm) originate from the absorption of benzene rings in PSS,[41] and the broad absorption bands in the visible and infrared regions are related to free charge carriers in PEDOT. The absorption characteristics around 900 nm are attributed to the polaron absorption of PEDOT ($PEDOT^{+}$), while the absorption characteristics above 970 nm are from the polaron absorption ($PEDOT^{++}$). In Figure 2d, the peaks at 600, 900, and 1100 nm are assigned to the neutral, polaron, and bipolar states of PEDOT, respectively.[39] As shown in Figure S3, the absorption intensity below 300 nm becomes lower after doping, indicating that PSS in the film is reduced after doping with DPM or PPH. The absorption intensity above 900 nm does not change much before and after doping, which means that the polaron and bipolaron states of PEDOT do not fluctuate much after DPM and PPH doping. Therefore, the UV−visible near-infrared results show that carrier concentration does not seem to be the main factor affecting the conductivity increase of PEDOT:PSS films after DPM or PPH doping, while the decrease in PSS is very important for the improvement of film conductivity.

To verify the reduction of PSS content after doping with DPM and PPH, X-ray photoelectron spectroscopy (XPS) was used to study and analyze the changes in the surface composition of the PEDOT:PSS films. As shown in Figure 3a, the fine spectrum of S 2p corresponds to the original and doped PEDOT:PSS, and Figure 3b shows the full spectrum. There is more than one peak signal in S 2p, which comes from the thiophene ring (PEDOT) and the counteranion (PSS), respectively, because they have different chemical environments. The blue part corresponds to the oxidation states of PEDOT and PEDOT ($PEDOT^{+}$). Due to some sulfonic acid groups from PEDOT electronic PSS, the red part corresponds to the charged PSS^{-} and the neutral PSSH, which has a high binding energy (from 166 to 171 eV) sulfur atom corresponding to PSS and a lower binding energy (from 162 to 165 eV) sulfur atom corresponding to PEDOT.[42]

Therefore, by integrating each peak in S 2p, the ratio of the peak area of PSS to PEDOT can be obtained, and then the content ratio of PSS to PEDOT can be calculated. The ratio between the two phases, after determining the integral area peak, is shown in Figure 3c. Without doping of PEDOT:PSS films, the PSS and PEDOT peak area ratio is about 2.26. In the doping of PEDOT:PSS films, it reduces to 1.75 and 1.85, respectively. Therefore, we can assume that due to the doping with DPM or PPH, the Coulomb electrostatic interaction between PEDOT and PSS weakens, promoting the phase separation of the two polymers.[43] In this process, it also leads

https://doi.org/10.1021/acsomega.3c09187
ACS Omega 2024, 9, 15040−15051

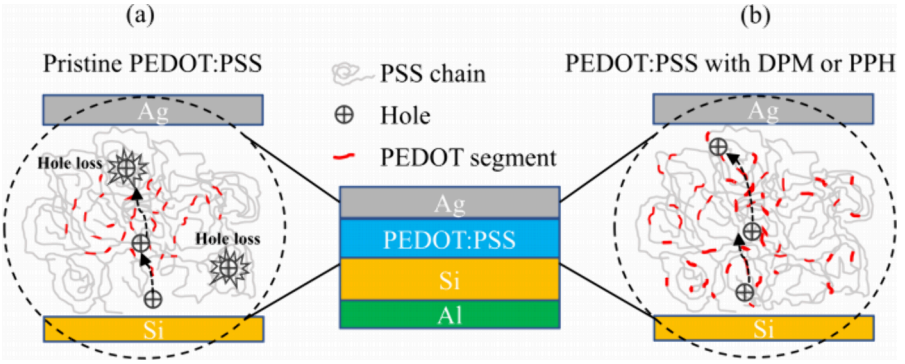

Figure 5. Schematic diagram of carrier transport in PEDOT:PSS films: (a) pristine and (b) doped with DPM or PPH.

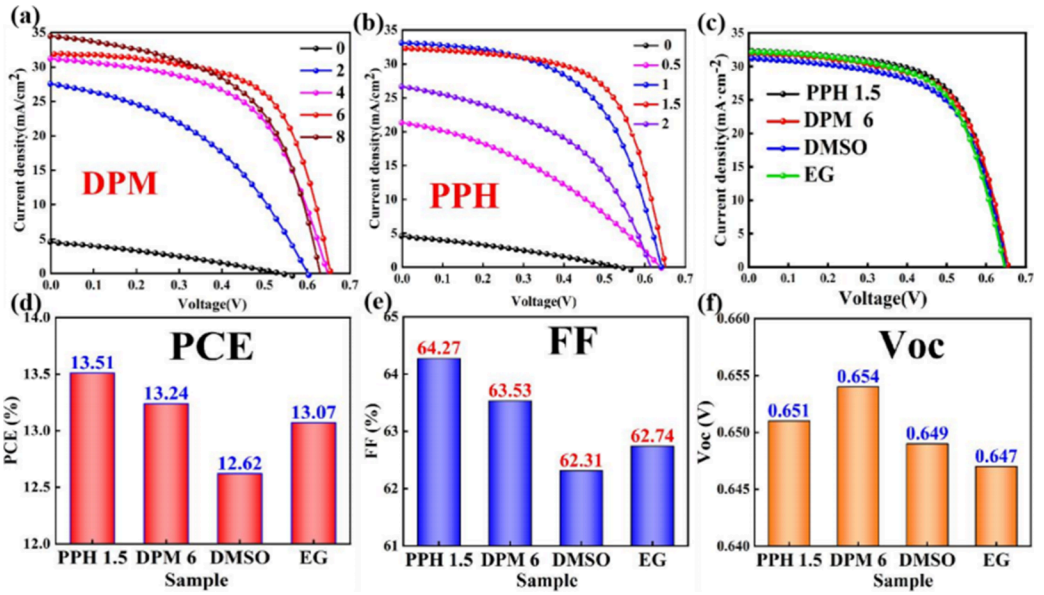

Figure 6. $J-V$ curves of solar cells doped with different solvents (different concentrations): (a) DPM and (b) PPH. (c) $J-V$ curves of solar cells doped with 6 wt % DPM, 1.5 wt % PPH, 5 wt % DMSO, and 7 wt % EG. Performance comparison of solar cells by doping with different solvents: (d) PCE, (e) FF, and (f) V_{oc}.

to the redistribution of PEDOT along the PSS chain, facilitating the "release" of free PSS. This contributes to the formation of more PEDOT-rich domains, enhancing the conductivity of the PEDOT:PSS film.[44] This result is mutually confirmed by a previous conclusion.

The chemical structure changes of PEDOT:PSS films before and after doping were characterized by Raman spectroscopy to explore the mechanism of the enhanced conductivity of PEDOT:PSS films caused by DPM or PPH doping. In Figure 4a, within the range from 440 to 1568 cm^{-1}, there is a peak in the undoped PEDOT:PSS film due to the carbon atom vibration. The peak at 1426 cm^{-1} is attributed to the C_α-C_β symmetric tensile vibration in the quinone structure, and the peak at 1435 cm^{-1} is attributed to the C_α-C_β symmetric tensile vibration in the PEDOT benzene structure. Additionally, there is a corresponding C_α-C_β asymmetric stretching mode at 1537 and 1568 cm^{-1}.[18,20]

In Figure 4b, upon doping with 6 wt % DPM or 1.5 wt % PPH, there is an obvious red shift of the peak from 1435 to 1426 cm^{-1}. This shift indicates the transformation from the benzene structure to the quinoid structure in the PEDOT molecule, as suggested by the symmetry of PEDOT alpha C_α-C_β stretching vibration.[39] The extent of conversion from the benzenoid structure to the quinoid structure is associated with a significant increase in the positive charge density of PEDOT, resulting in a broader peak at 1426 cm^{-1}. Simultaneously, it is observed that with the incorporation of DPM and PPH, the ratio of the peak intensity at 1505 cm^{-1} to the peak intensity at 1426 cm^{-1} decreases, implying a reduction in the PEDOT content with the benzene structure.[18] Therefore, after the doping with DPM or PPH, the linear quinone structures of PEDOT increase.

Related studies have shown that PEDOT with a benzene structure has poor conductivity and is prone to exist as a coil in PEDOT:PSS films. However, PEDOT with a quinoid structure is stretched into a linear or fibrous character, which is the primary reason for its higher conductivity.[20,41] As depicted in Figure 4c, the benzene structure undergoes transformation to a quinone structure. The conversion of a single bond to a double bond makes it difficult to rotate the rings in PEDOT, increasing the rigidity of PEDOT with a quinone structure compared to the benzene structure. The enhancement of the degree of π electron delocalization in the main chain of the linear structure contributes to the increased electrical conductivity of PEDOT:PSS films.[45−47] The results of the Raman analysis indicate that the transformation of the PEDOT

https://doi.org/10.1021/acsomega.3c09187
ACS Omega 2024, 9, 15040−15051

chain from benzene to a quinone structure in PEDOT:PSS induced by DPM or PPH doping is one of the reasons for the improved conductivity of PEDOT:PSS films.

Figure 5 presents a more intuitive schematic illustration explaining the significant increase in the conductivity of PEDOT:PSS films after doping with DPM and PPH. As depicted in Figure 5a, the conductive and hydrophobic PEDOT is uniformly distributed inside the PEDOT:PSS grain with the insulating and hydrophilic PSS surrounding the exterior. In this structural configuration, the insulating PSS reduces the film's conductivity because the outer insulating region hinders carrier transport.[48] In Figure 5b, postdoping with DPM or PPH results in the internal separation of the PEDOT chain from the PSS chain. The PEDOT concentrated inside the grain is radially and uniformly distributed from the grain center, establishing a continuous conductive pathway. This configuration enhances the overall conductivity of the PEDOT:PSS film.

2.3. DPM and PPH Doping Improves the Performance of Si/PEDOT:PSS Solar Cells. We investigated the effect of doping with DPM or PPH on the performance of Si/PEDOT:PSS solar cells. The size of the solar cells we prepared is 1.1 × 1.1 cm^2. Under standard solar illumination, the performance parameters of DMSO, EG, and the original Si/PEDOT:PSS solar cells with varying concentrations of DPM and PPH are comprehensively presented in Table S2. The corresponding $J-V$ curves are depicted in Figure 6a−c. In Table 1, we compare the PCE of Si/PEDOT:PSS solar cells corresponding to the optimal doping amounts of different solvents.

Table 1. Performance of Solar Cells by Doping with Different Solvents

sample	V_{oc} (V)	J_{sc}(mA/cm^2)	FF (%)	PCE (%)
control	0.539	4.59	30.38	0.74
M 6	0.654	31.87	63.53	13.24
H 1.5	0.651	32.28	64.27	13.51
DMSO	0.649	31.21	62.31	12.62
EG	0.647	32.19	62.74	13.07

The PCE of the original solar cell is only 0.74%, with a short-circuit current density (J_{sc}) of 4.59 mA/cm^2, an open circuit voltage (V_{oc}) of 539 mV, and a fill factor (FF) of 30.38%. As concluded earlier, this is attributed to the low conductivity of the original PEDOT:PSS film. Following the doping with DPM and PPH, the PCE of the PEDOT:PSS/Si solar cell significantly improved. However, the PCE of the device is correlated with the doping concentration. In Figure S4, after doping with DPM and PPH, J_{sc}, FF, V_{oc}, and PCE exhibit notable increases. The optimal performance is achieved at 6 wt % DPM and 1.5 wt % PPH, after which these parameters begin to decline. Specifically, for DPM doping, the optimal performance includes J_{sc} = 31.87 mA/cm^2, V_{oc} = 654 mV, FF = 63.53%, and PCE = 13.24%. For PPH doping, optimal performance is observed with J_{sc} = 32.28 mA/cm^2, V_{oc} = 651 mV, FF = 64.27%, and PCE = 13.51%. The champion efficiency, represented by PCE values, is recorded for each type of solar cell in Figure S5, with 10 solar cell devices being used for each type. The external quantum efficiency (EQE) spectrum for Si/PEDOT:PSS solar cells with DPM and PPH doping was measured (Figure S6), and the obtained short-circuit current is consistent with our test results. The original solar cell is not shown in the figure due to the inability to obtain EQE. The factors contributing to the improvement of these parameters are primarily determined by the structure of PEDOT:PSS, the photoelectric properties of the films, and the quality of the Si/PEDOT:PSS heterojunctions formed.

It should be noted that the effect of DPM and PPH doping of PEDOT:PSS is superior to that with commonly used DMSO and EG, where the solvents doped with PEDOT:PSS are DMSO and EG. Table 1 provides a comparison of the PCE of Si/PEDOT:PSS solar cells with different optimal doping amounts of the solvents. It can be seen that the performance of solar cells using DMSO- and EG-doped PEDOT:PSS is not equal to that of DPM or PPH doping. The PCEs of solar cell devices doped with DMSO and EG are only 12.62 and 13.07%, respectively. The $J-V$ curve of doping with four solvents is illustrated in Figure 6c, with the intersection point between the curve and the horizontal axis depicted in Figure S7. In Figure 6d−f, the optimal doping amount corresponding to PCE, FF, and V_{oc} is contrasted for the four doping solvents. DPM- or PPH-doped solar cells exhibit a higher PCE due to increased FF and V_{oc}.

To investigate the reason for the significant increase in the level of V_{oc} before and after doping with DPM or PPH, electrochemical impedance tests and dark current tests were performed. Figure 7a displays the electrochemical impedance spectroscopy (EIS) diagram of the Si/PEDOT:PSS solar cell, both before and after doping with 6 wt % DPM and 1.5 wt % PPH into the PEDOT:PSS film. The Nyquist diagram enables the exploration of processes, such as material transfer, charge transfer, and diffusion in the solar cell. It also allows the calculation of resistance or capacitance values that affect the solar cell system.[49] Illustrations of the schematic circuit simulation include series resistance (R_s), composite resistance (R_P), and composite capacitance equivalent (C_{PE}) circuit diagrams (Figure 7a).

For all Si/PEDOT:PSS solar cells (prepared under the same conditions), the resistance values of the metal electrodes (Ag electrodes on the front and Al electrodes on the back) and Si sheets are expected to be the same. R_s mainly depends on the conductive properties of the PEDOT:PSS layer, Ag/PEDOT:PSS, and Si/PEDOT:PSS interfaces. As mentioned above, PEDOT:PSS doped with DPM and PPH will alter the Coulomb electrostatic interaction between PEDOT and PSS, generate more conductive PEDOT chains, and form more efficient Ag/PEDOT:PSS and PEDOT:PSS/Si contact interfaces, thereby reducing the resistance. As shown in Figure 7b, the R_s of Si/PEDOT:PSS solar cells is reduced after doping with DPM or PPH, corresponding to the increasing trend of PCE in solar cells. Table S3 displays the fitted parameters. In comparison with the original device, the R_s values for DPM or PPH doping are 3.78, 4.47, and 4.96 Ohm, respectively. This implies that the conductivity of PEDOT:PSS is improved, and the contact resistance is reduced due to doping-enhanced carrier separation and transport.[50]

Minority carrier lifetime (MCLT) represents the minimum time for recombination of photogenerated charge carriers (holes and electrons), directly influencing the quality, surface properties, device processing, and design of silicon materials.[51] Both the bulk and surface recombination of charge carriers affect MCLT values. However, since the carrier lifetime caused by the bulk component is much larger than the surface component, the measured effective MCLT represents the surface composite lifetime contributed by the two surfaces of

https://doi.org/10.1021/acsomega.3c09187
ACS Omega 2024, 9, 15040−15051

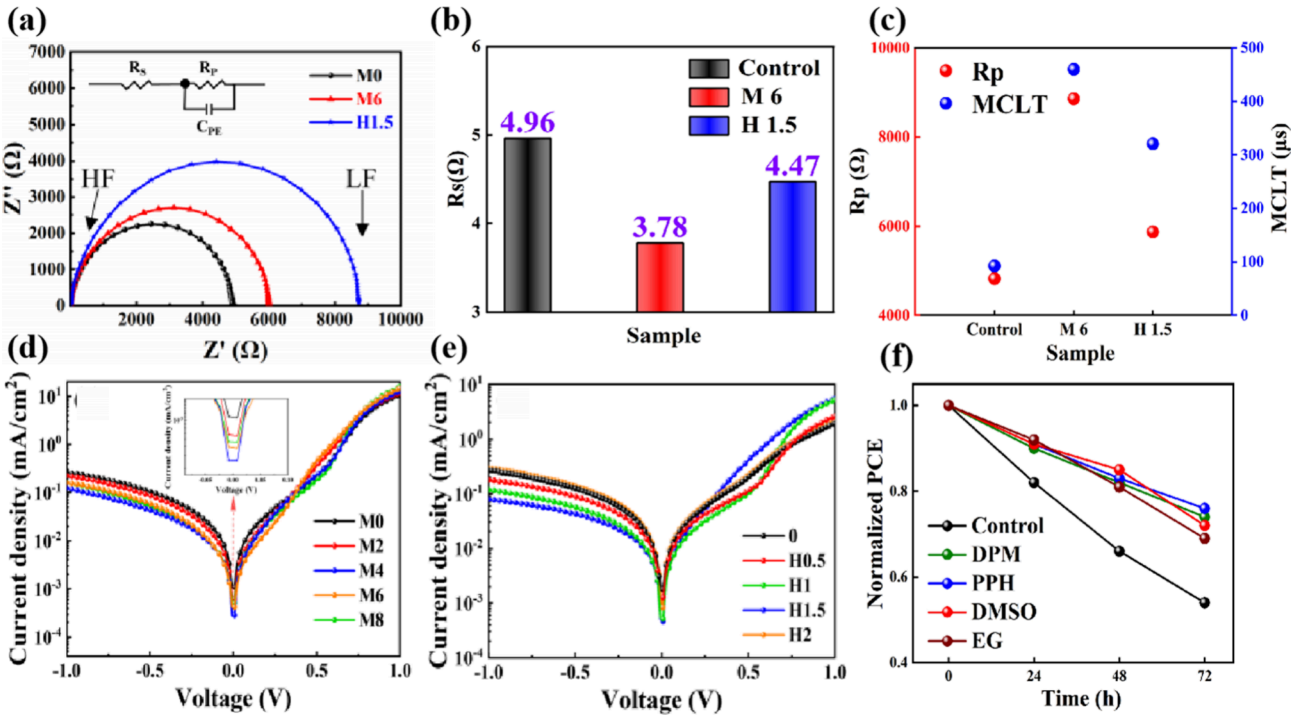

Figure 7. (a) EIS and (b) series resistance (R_s) of the Si/PEDOT:PSS solar cells: original and doped with 6 wt % DPM or 1.5 wt % PPH. (c) The composite resistor and MCLT were obtained by fitting of the original solar cells and solar cells doped with 6 wt % DPM or 1.5 wt % PPH. Dark $J-V$ curves of the PEDOT:PSS/Si solar cell by doping with (d) DPM and (e) PPH. (f) Stability test of original solar devices and solar devices doped with 6 wt % DPM or 1.5 wt % PPH in an air environment (the temperature is 22 °C, and the humidity is 50%).

the silicon wafer.[52,53] The carrier life (τ) of the Si/PEDOT:PSS solar cell is calculated according to the formula: $\tau = R_p \times C_{PE}$, where RP is the composite resistance and CPE is the capacitive resistance.[49] In all experiments, similar electronic (doping type, density) and surface properties (thickness, texture, surface defect status, etc.) of silicon wafers are utilized. Table S3 displays the minority carrier lifetimes of the original and after doping with DPM and PPH as 92.31, 459.86, and 320.43 μs, respectively. The comparison of the minority carrier lifetime of the original and after doping with the optimal concentration of DPM and PPH is shown in Figure 7c.

During the formation of heterojunctions at the PEDOT:PSS/Si interface, the strong electric field generated may lead to an increase in the density of holes (minority carriers) near the Si surface, resulting in the formation of an inverted layer (where the hole concentration may be higher than that of electrons in the bulk silicon wafer). Consequently, a stronger electric field leads to a lower electron density near the Si surface, resulting in a higher MCLT value. In simpler terms, higher MCLT values indicate a more pronounced PEDOT:PSS/Si interface, generating a larger electric field. MCLT measurements also confirmed that PEDOT:PSS can passivate the textured Si surface state. After addition of DPM or PPH, MCLT values of PEDOT:PSS films increase, indicating a significant reduction in surface defects after doping. Additionally, the analysis of MCLT reveals that heterojunctions with good structural quality are formed at the Si/PEDOT:PSS interface, inhibiting the recombination of minority carriers.[11,54]

Composite resistance (R_P) is a key factor in PEDOT:PSS/Si solar cells, as it can be used to analyze carrier loss.[50] The low recombination obviously provides a longer charge carrier lifetime. As shown in Figure 7c, the R_P of solar cells doped with 6 wt % DPM or 1.5 wt % PPH changes from 4822 Ω to 8860 Ω and 5871 Ω compared to the original. The strong inversion effect resulted in a relatively high CPE, which changed from 191.44 nF to 519.03 nF and 545.79 nF.

The improvement in V_{oc} can be verified by the dark $J-V$ characteristics. The dark-state $J-V$ curves of Si/PEDOT:PSS solar cells doped with DPM and PPH at different concentrations are shown in Figure 7d,e. A higher photocurrent and dark current density ratio (J_{sc}/J_0) can result in a higher V_{oc}. This relation for V_{oc} is given by the two equations, $V_{oc} = \frac{KT}{q}\ln\left(\frac{J_{sc}}{J_0} + 1\right)$ and $J_{dark}(V) = J_0\left[\exp\left(\frac{qV}{nkT}\right) - 1\right]$, where q is the electron charge, K is Boltzmann's constant, n is the ideality factor, and T is the temperature.[55] Hence, the increase in V_{oc} is attributed to the increase in the concentration of J_{sc}/J_0. Therefore, with DPM 6 and PPH 1.5 doping, PEDOT:PSS obtains a higher J_{sc}/J_0, resulting in the highest V_{oc} for Si/PEDOT:PSS HSCs at 654 and 651 mV.

The Si/PEDOT:PSS solar cells have the smallest J_0 when the concentrations of doped DPM and PPH are 6 and 1.5 wt %, respectively, corresponding to V_{oc} of 654 and 651 mV, respectively. Meanwhile, the PCEs of solar cell devices reach 13.24 and 13.51%, respectively. The dark-state $J-V$ curve shows that a higher concentration of doping will lead to a larger leakage flow of solar cells. This may be because a higher concentration of DPM or PPH doping will worsen the quality of the PEDOT:PSS film and increase internal defects.[56] The original PEDOT:PSS thin film solar cell, due to the presence of more recombination centers, leads to more complex loss and therefore shows a low V_{oc}. The high V_{oc} obtained after doping with DPM and PPH indicates that doping improves junction formation and surface passivation (reducing the surface

https://doi.org/10.1021/acsomega.3c09187
ACS Omega 2024, 9, 15040−15051

recombination of charge carriers) on the silicon surface. This is consistent with the results of the previous EIS analysis.

In addition, we also conducted an air stability exploration of Si/PEDOT:PSS solar cells doped with DPM, PPH, DMSO, and EG and original solar cells, as shown in Figure 7g. The five groups of solar cell devices were placed in an air environment with a temperature of 22.0 °C and a humidity of 50%. After 72 h, the PCE of the original (control) solar cell devices dropped to 54% of the initial value. However, the PCEs of solar cell devices doped with DPM, PPH, DMSO, and EG were 74, 76, 72, and 69% of the initial value, respectively, after 72 h. This indicates that the air stability of the solar cell device can be significantly improved after doping and suggests that the solar cell device doped with DPM and PPH is comparable to that of the device doped with DMSO and EG.

2.4. Discussion. The performance of solar cells is not only related to the quality of silicon wafers but also related to the photoelectric performance of the PEDOT:PSS film. The original PEDOT:PSS films showed poor photoelectric performance, such as low conductivity, carrier concentration, and poor infiltration with silicon wafers. The photoelectric performance of PEDOT:PSS films doped with DPM or PPH was greatly improved. It would make a significant contribution to the PCE of solar cells. The PCE of Si/PEDOT:PSS solar cells was from 0.74% to 13.24% (DPM) and 13.51% (PPH). To obtain solar cells with a higher PCE, we can also use alkaline or acidic solutions for etching on silicon wafers to obtain nanostructures, such as pyramids or nanowires. By reduction of the reflection of light, the PCE of solar cells can further improve.

3. CONCLUSIONS

We investigated the effects of DPM and PPH doping on the microscopic morphology and photoelectric properties of PEDOT:PSS films as well as the optimal concentration of DPM- and DPH-doped PEDOT:PSS films. The reduction of PSS content and the transformation of the PEDOT chain from benzene to a quinone structure in PEDOT:PSS induced by DPM or PPH doping are the reasons for the improved conductivity of PEDOT:PSS films. Doping with DPM and DPH not only increased the conductivity of the original film (0.015 S/cm) to 746.27 S/cm (DPM) and 710.21 S/cm (PPH) but also improved the PCE of Si/PEDOT:PSS solar cells from 0.74% to 13.24% (DPM) and 13.51% (PPH). Modified PEDOT:PSS with DPM and PPH can improve junction formation and surface passivation, reducing the surface recombination of charge carriers on the silicon surface. Additionally, the air stability and PCE of Si/PEDOT:PSS solar cells doped with DPM (13.24%), DPH (13.51%), ethylene glycol (EG, 13.07%), and dimethyl sulfoxide (DMSO, 12.62%) were compared. We concluded that the use of DPM and DPH doping can replace the solvents DMSO and EG, often used in doping modified PEDOT:PSS. Compared to DMSO and EG, DPM and DPH are more economical and environmentally friendly, helping to reduce the manufacturing cost of Si/PEDOT:PSS solar cells and making them more conducive to commercial applications.

4. EXPERIMENTAL SECTION

4.1. Methods and Materials. Dipropylene glycol methyl ether ($C_7H_{16}O_3$, DPM, 99%, BR, Macklin), propylene glycol phenyl ether ($C_9H_{12}O_2$, PPH, >98%, Guangdong Runhong Chemical), dimethyl sulfoxide (DMSO, 99.9%, Aladdin), ethylene glycol (EG, 99.9%, Aladdin), Triton X-100 (Sigma-Aldrich), PEDOT:PSS (Clevis PH1000), and *n*-Si (resistivity, 0.05−0.1 Ω cm; orientation, ⟨100⟩; one-side polished; thickness of 300 ± 10 μm; Suzhou Research Materials Microtech Co., Ltd.) were used in this study.

4.2. Fabrication of Si/PEDOT:PSS Solar Cells. *4.2.1. Preparation of the PEDOT:PSS Predispersion Solution.* PEDOT:PSS is a liquid. On the clean experimental glass bottles, they are labeled successively with labels M0 (control, original), M2, M4, M6, M8, H0.5, H1, H1.5, and H2 (M stands for DPM, H stands for PPH, and the number after the letter indicates the mass percentage of PEDOT:PSS; for example, M2 represents 2 wt % DPM added). PEDOT:PSS dispersions were weighed 1 g each time using an electronic balance and added to the above glass bottles, and then DPM (0.02 to 0.08 g) and PPH (0.005 to 0.02 g) were weighed in turn. Original and DMSO- and EG-doped samples were set as the control group. PEDOT:PSS was mixed with 5 wt % DMSO and 7 wt % EG and added to each glass bottle. Triton X-100 (0.002 g) was continued to weigh each time and added in turn, and then the mixture was put and moved to the magnetic stirrers. The mixture was stirred at 300 rpm for 10 h at room temperature before use.

4.2.2. Cleaning of Si Slices. The larger Si slices were cut into several 1.1 × 1.1 cm^2 squares and sonicated with acetone and absolute ethanol for 15 min in turn. The purpose was to clean and remove the organic matter attached to the Si surface. Then, ultrasonication was performed twice with deionized water for 5 min each time. Then, the Si sheet was transferred to a dilute solution of 10% hydrofluoric acid (HF), and the immersion time was 180s. Then, the Si sheet was sonicated with deionized water twice and once for 5 min. After this step of cleaning, the natural oxides on the Si surface were removed. Finally, the deionized water was sonicated twice and sealed with absolute ethanol solution until use.

4.2.3. Spin-Coating the Predispersion of PEDOT:PSS on Si. The cleaned Si slices were blown dry with N_2, and the PEDOT:PSS predispersion was coated on the Si slices using a spin-coating instrument in a glovebox at a rotation speed of 2500 rpm (spin-coating time of 55 s) and annealed at 130 °C for 15 min.

4.2.4. Preparation of Electrodes. A 180 nm-thick Ag top electrode and 55 nm-thick Al back electrode were deposited at 0.2 and 0.1 nm/s at a vacuum of 5 × 10^{-4} Pa by thermal evaporation of high-purity metal using a high vacuum coating instrument.

4.3. Test of Si/PEDOT:PSS Solar Cells. The size of the solar cells we prepared is 1.1 × 1.1 cm^2. A solar simulator (AM 1.5) with an intensity of 100 mW/cm^2 was used to imitate natural sun illumination and assess the current density−voltage (J−V) relationship.

4.4. Characterization. The surface morphology of the PEDOT:PSS thin films was measured by scanning electron microscopy (SEM, Nova Nano SEM 450) and atomic force microscopy (AFM, SPI-3800). The contact angle was measured by SINDIN SDC-200S (Dongguan Shengding Precision). The electrical characteristic parameters (conductivity and carrier concentration of different modified PEDOT:PSS films) were obtained through the Hall effect test (ET900 Hall effect test system). Absorbance and transmittance were measured by a UV−vis spectrophotometer (UV 2600). The valence state of PEDOT:PSS thin films was

https://doi.org/10.1021/acsomega.3c09187
ACS Omega 2024, 9, 15040−15051

determined by X-ray photoelectron spectroscopy (XPS, K-Alpha+). Raman spectra were measured by a Raman spectrometer (LabRAM HR, Horiba of Japan). Electrochemical impedance spectroscopy (EIS) was performed using an electrochemical workstation (CHI660E, Shanghai Chen Hua). EIS was carried out at room temperature in a frequency range of 1 Hz to 1 MHz with an AC amplitude of 10 mV. The solar simulator (AM 1.5) with an intensity of 100 mW/cm^2 was used to imitate natural sun illumination and assess the current density−voltage (J−V) relationship (using the Zolix solar test equipment, Keithley 2400 Source Meter). The quantum efficiency measurement system (ZolixSCS150) was employed for external quantum efficiency (EQE). The test was performed using a xenon light source with a wavelength range of 300−1100 nm. Partial equipment details can be found in the Advanced Analysis and Measurement Center of Yunnan University.

■ ASSOCIATED CONTENT

Supporting Information

The Supporting Information is available free of charge at https://pubs.acs.org/doi/10.1021/acsomega.3c09187.

More information about the physical and chemical changes after DPM and PPH doping of PEDOT:PSS and corresponding performance of the solar cell (PDF)

■ AUTHOR INFORMATION

Corresponding Authors

Juan Wang − *International Joint Research Center for Optoelectronic and Energy Materials, School of Materials and Energy, Yunnan University, Kunming, Yunnan 650091, China*; Email: wjuan0130@ynu.edu.cn

Xiaoming Wen − *School of Science, RMIT University, Melbourne, VIC 3000, Australia*; orcid.org/0000-0001-8298-483X; Email: xiaoming.wen@rmit.edu.au

Yu Yang − *International Joint Research Center for Optoelectronic and Energy Materials, School of Materials and Energy, Yunnan University, Kunming, Yunnan 650091, China*; orcid.org/0000-0002-7802-3654; Email: yuyang@ynu.edu.cn

Authors

Guijun Zhang − *International Joint Research Center for Optoelectronic and Energy Materials, School of Materials and Energy, Yunnan University, Kunming, Yunnan 650091, China*

Hua Peng − *International Joint Research Center for Optoelectronic and Energy Materials, School of Materials and Energy, Yunnan University, Kunming, Yunnan 650091, China*

Qianwen Wei − *International Joint Research Center for Optoelectronic and Energy Materials, School of Materials and Energy, Yunnan University, Kunming, Yunnan 650091, China*

Zheng Zhou − *International Joint Research Center for Optoelectronic and Energy Materials, School of Materials and Energy, Yunnan University, Kunming, Yunnan 650091, China*

Haixia Wu − *International Joint Research Center for Optoelectronic and Energy Materials, School of Materials and Energy, Yunnan University, Kunming, Yunnan 650091, China*

Jingjing Luo − *International Joint Research Center for Optoelectronic and Energy Materials, School of Materials and Energy, Yunnan University, Kunming, Yunnan 650091, China*

Complete contact information is available at: https://pubs.acs.org/10.1021/acsomega.3c09187

Notes

The authors declare no competing financial interest.

■ ACKNOWLEDGMENTS

The authors gratefully acknowledge financial support from the funds for leading local scientific-technological development by the central government (no. 202307AB110010) and the Yunling Scholars Fund of Yunnan Province Xing Dian Talents Program (no. KC194317). We appreciate the sample testing services provided by the Advanced Analysis and Measurement Center of Yunnan University.

■ REFERENCES

(1) Krebs, F. C. Fabrication and processing of polymer solar cells: A review of printing and coating techniques. *Sol. Energy Mater. Sol. Cells* **2009**, *93* (4), 394−412.

(2) Srivastava, A.; Sharma, R. K.; Sharma, D.; Tawale, J. S.; Agrawal, V. V.; Srivastava, S. K. Unveiling the role of ethylene glycol for enhanced performance of PEDOT:PSS/Silicon hybrid solar cells. *Opt. Mater.* **2022**, *134*, No. 112922, DOI: 10.1016/j.optmat.2022.112922.

(3) Srivastava, A.; Sharma, R. K.; Sharma, D.; Kumari, P.; Agrawal, V. V.; Srivastava, S. K. Influence of alcoholic polar surfactants on PEDOT:PSS for enhanced performance of organic/Si hybrid solar cell. *Surf. Interfaces* **2023**, *38*, No. 102822, DOI: 10.1016/j.surfin.2023.102822.

(4) Singh, P.; Srivastava, S. K.; Sivaiah, B.; Laxmi, S.; Prathap, P.; Rauthan, C. M. S. Light intensity dependent characteristics of micro-textured Si/PEDOT:PSS heterojunction solar cell. *J. Mater. Sci. Mater. Electron.* **2018**, *29* (6), 5087−5097.

(5) Cao, R.; Gao, Z.; Cui, M.; Liu, W.; Zhang, Y.; Luo, Y.; Chen, L.; Li, Y.; Li, M. Research progress of Si/PEDOT:PSS hybrid solar cells. *J. Funct. Mater.* **2019**, *50* (1), 1006 DOI: 10.3969/j.issn.1001-9731.2019.01.002.

(6) Yu, L.-M.; Man, J.-X.; Chen, T.; Luo, D.; Wang, J.; Yang, H.; Zhao, Y.-B.; Wang, H.; Yang, Y.; Lu, Z.-H. Colorful conducting polymers for vivid solar panels. *Nano Energy* **2021**, *85*, No. 105937, DOI: 10.1016/j.nanoen.2021.105937.

(7) Liu, R.; Sun, B. Silicon-based Organic/inorganic Hybrid Solar Cells. *Acta Chimica Sinica* **2015**, *73* (3), 225−236.

(8) Thomas, J. P.; Leung, K. T. Defect-Minimized PEDOT:PSS/Planar-Si Solar Cell with Very High Efficiency. *Adv. Funct. Mater.* **2014**, *24* (31), 4978−4985.

(9) Wang, J.; Zhou, W.; Wei, Q.; Liu, G.; Yuan, X.; Pen, H.; Zhang, G.; Wang, R.; Wang, C.; Yang, Y. Effect of Au@MoS_2 Contacted PEDOT:PSS on Work Function of Planar Silicon Hybrid Solar Cells. *Adv. Mater. Interfaces* **2023**, *10*, 2300187 DOI: 10.1002/admi.202300187.

(10) Yoon, S.-S.; Khang, D.-Y. High Efficiency (>17%) Si-Organic Hybrid Solar Cells by Simultaneous Structural, Electrical, and Interfacial Engineering via Low-Temperature Processes. *Adv. Energy Mater.* **2018**, *8* (9), 1702655 DOI: 10.1002/aenm.201702655.

(11) He, J.; Gao, P.; Yang, Z.; Yu, J.; Yu, W.; Zhang, Y.; Sheng, J.; Ye, J.; Amine, J. C.; Cui, Y. Silicon/Organic Hybrid Solar Cells with 16.2% Efficiency and Improved Stability by Formation of Conformal Heterojunction Coating and Moisture-Resistant Capping Layer. *Adv. Mater.* **2017**, *29* (15), 1606321 DOI: 10.1002/adma.201606321.

(12) Lin, G.; Gao, Z.; Gao, T.; Chen, Y.; Geng, Q.; Li, Y.; Chen, L.; Li, M. Research progress in improving the performance of

PEDOT:PSS/Micro- and Nano-textured Si heterojunction for hybrid solar cells. *J. Materiomics* **2021**, *7* (5), 1161−1179.
(13) Guo, H.; Chen, T.; Yu, L.; Chen, A.; Sun, T.; Wang, J.; Wang, C.; Zhang, J.; Yang, Y. Enhanced performance of Si/PEDOT: PSS heterojunction solar cells via multi-walled carbons coated with polydopamine. *Opt. Mater.* **2021**, *120*, No. 111375, DOI: 10.1016/j.optmat.2021.111375.
(14) Khang, D.-Y. Recent progress in Si-PEDOT:PSS inorganic organic hybrid solar cells. *J. Phys. D: Appl. Phys.* **2019**, *52* (50), 503002 DOI: 10.1088/1361-6463/ab3f64.
(15) Sun, Z.; He, Y.; Xiong, B.; Chen, S.; Li, M.; Zhou, Y.; Zheng, Y.; Sun, K.; Yang, C. Performance-Enhancing Approaches for PEDOT:PSS-Si Hybrid Solar Cells. *Angew. Chem., Int. Ed.* **2021**, *60* (10), 5036−5055.
(16) Zhou, W.; Zhang, H.; Wang, J.; Wei, Q.; Chen, Z.; Wang, C.; Yang, Y. High conductivity PEDOT:PSS thin films affording improved open circuit voltages in PEDOT:PSS-Si heterojunction solar cells. *Mater. Lett.* **2022**, *312*, No. 131466, DOI: 10.1016/j.matlet.2021.131466.
(17) Chi, D.; Qi, B.; Wang, J.; Qu, S.; Wang, Z. High-performance hybrid organic-inorganic solar cell based on planar n-type silicon. *Appl. Phys. Lett.* **2014**, *104* (19), 193903 DOI: 10.1063/1.4875913.
(18) Yu, L.-M.; Chen, T.; Feng, N.; Wang, R.; Sun, T.; Zhou, Y.; Wang, H.; Yang, Y.; Lu, Z.-H. Highly Conductive and Wettable PEDOT:PSS for Simple and Efficient Organic/c-Si Planar Heterojunction Solar Cells. *Sol. RRL* **2020**, *4* (4), 1900513 DOI: 10.1002/solr.201900513.
(19) Thomas, J. P.; Srivastava, S.; Zhao, L.; Abd-Ellah, M.; McGillivray, D.; Kang, J. S.; Rahman, M. A.; Moghimi, N.; Heinig, N. F.; Leung, K. T. Reversible Structural Transformation and Enhanced Performance of PEDOT:PSS-Based Hybrid Solar Cells Driven by Light Intensity. *ACS Appl. Mater. Interfaces* **2015**, *7* (14), 7466−7470.
(20) Thomas, J. P.; Zhao, L.; McGillivray, D.; Leung, K. T. High-efficiency hybrid solar cells by nanostructural modification in PEDOT:PSS with co-solvent addition. *J. Mater. Chem. A* **2014**, *2* (7), 2383−2389.
(21) Liu, Q.; Ishikawa, R.; Funada, S.; Ohki, T.; Ueno, K.; Shirai, H. Highly Efficient Solution-Processed Poly(3,4-ethylenedioxythiophene):Poly(styrenesulfonate)/Crystalline-Sil icon Heterojunction Solar Cells with Improved Light-Induced Stability. *Adv. Energy Mater.* **2015**, *5* (17), 1500744 DOI: 10.1002/aenm.201500744.
(22) Pietsch, M.; Bashouti, M. Y.; Christiansen, S. The Role of Hole Transport in Hybrid Inorganic/Organic Silicon/Poly(3,4-ethylenedioxy-thiophene):Poly(styrenesulfonate) Heterojunction Solar Cells. *J. Phys. Chem. C* **2013**, *117* (18), 9049−9055.
(23) Thomas, J. P.; Leung, K. T. Mixed co-solvent engineering of PEDOT:PSS to enhance its conductivity and hybrid solar cell properties. *J. Mater. Chem. A* **2016**, *4* (44), 17537−17542.
(24) Yu, Z.; Xia, Y.; Du, D.; Ouyang, J. PEDOT:PSS Films with Metallic Conductivity through a Treatment with Common Organic Solutions of Organic Salts and Their Application as a Transparent Electrode of Polymer Solar Cells. *ACS Appl. Mater. Interfaces* **2016**, *8* (18), 11629−11638.
(25) Zhu, Z.; Liu, C.; Xu, J.; Jiang, Q.; Shi, H.; Liu, E. Improving the Electrical Conductivity of PEDOT:PSS Films by Binary Secondary Doping. *Electron. Mater. Lett.* **2016**, *12* (1), 54−58.
(26) Shahrim, N. A. A.; Ahmad, Z.; Azman, A. W.; Buys, Y. F.; Sarifuddin, N. Mechanisms for doped PEDOT:PSS electrical conductivity improvement. *Mater. Adv.* **2021**, *2* (22), 7118−7138.
(27) Chen, Y.; Meng, J.; Xu, Y.; Li, Y.; Zhang, Q.; Hou, C.; Sun, H.; Wang, G.; Wang, H. Integrated Ionic-Additive Assisted Wet-Spinning of Highly Conductive and Stretchable PEDOT:PSS Fiber for Fibrous Organic Electrochemical Transistors. *Adv. Electron. Mater.* **2021**, *7* (8), 2100231 DOI: 10.1002/aelm.202100231.
(28) Fowles, J.; Banton, M.; Klapacz, J.; Shen, H. A toxicological review of the ethylene glycol series: Commonalities and differences in toxicity and modes of action. *Toxicol. Lett.* **2017**, *278*, 66−83.
(29) Loriaux, D.; Bergin, S. P.; Patel, S. M.; Tucker, J.; Barkauskas, C. E. Ethylene Glycol Toxicity in the Setting of Recurrent Ingestion: A Case Report and Literature Review. *Cureus* **2019**, *11* (4), e4375 DOI: 10.7759/cureus.4375.
(30) Yue, H.; Zhao, Y.; Ma, X.; Gong, J. Ethylene glycol: properties, synthesis, and applications. *Chem. Soc. Rev.* **2012**, *41* (11), 4218−4244.
(31) Galvao, J.; Davis, B.; Tilley, M.; Normando, E.; Duchen, M. R.; Cordeiro, M. F. Unexpected low-dose toxicity of the universal solvent DMSO. *Faseb Journal* **2014**, *28* (3), 1317−1330.
(32) Willson, J. E.; Brown, D. E.; Timmens, E. K. A TOXICOLOGIC STUDY OF DIMETHYL SULFOXIDE. *Toxicol. Appl. Pharmacol.* **1965**, *7*, 104−12.
(33) Fairhurst, S.; Knight, R.; Marrs, T. C.; Scawin, J. W.; Spurlock, M. S.; Swanston, D. W. Percutaneous toxicity of ethylene glycol monomethyl ether and of dipropylene glycol monomethyl ether in the rat. *Toxicology* **1989**, *57* (2), 209−15.
(34) Cragg, S. T.; Boatman, R. J. Glycol Ethers: Ethers of Propylene, Butylene Glycols, and Other Glycol Derivatives. *Patty's Toxicol.* **2001**, 789 DOI: 10.1002/0471435139.tox087.
(35) Ouyang, L.; Musumeci, C.; Jafari, M. J.; Ederth, T.; Inganas, O. Imaging the Phase Separation Between PEDOT and Polyelectrolytes During Processing of Highly Conductive PEDOT:PSS Films. *ACS Appl. Mater. Interfaces* **2015**, *7* (35), 19764−19773.
(36) Gueye, M. N.; Carella, A.; Faure-Vincent, J.; Demadrille, R.; Simonato, J.-P. Progress in understanding structure and transport properties of PEDOT-based materials: A critical review. *Prog. Mater. Sci.* **2020**, *108*, No. 100616, DOI: 10.1016/j.pmatsci.2019.100616.
(37) Anitha, R.; Menon, S. S.; Bhalerao, G.; Siddham, P.; Baskar, K.; Singh, S. Electrical properties of nitric acid and DMSO treated PEDOT:PSS/n-Si hybrid heterostructures for optoelectronic applications. *J. Appl. Polym. Sci.* **2020**, *137* (32), 48952 DOI: 10.1002/app.48952.
(38) Gharahcheshmeh, M. H.; Gleason, K. K. Texture and nanostructural engineering of conjugated conducting and semiconducting polymers. *Mater. Today Adv.* **2020**, *8*, No. 100086, DOI: 10.1016/j.mtadv.2020.100086.
(39) Wang, C.; Sun, K.; Fu, J.; Chen, R.; Li, M.; Zang, Z.; Liu, X.; Li, B.; Gong, H.; Ouyang, J. Enhancement of Conductivity and Thermoelectric Property of PEDOT:PSS via Acid Doping and Single Post-Treatment for Flexible Power Generator. *Adv. Sustainable Syst.* **2018**, *2* (12), 1800085 DOI: 10.1002/adsu.201800085.
(40) Zhou, X.; Dong, X.; Liu, Y.; Wang, W.; Wei, W.; Chen, J.; Liu, T.; Zhou, Y. Effect of Wetting Surfactants on the Work Function of PEDOT:PSS for Organic Solar Cells. *ACS Appl. Energy Mater.* **2022**, *5* (3), 3766−3772.
(41) Kim, N.; Kee, S.; Lee, S. H.; Lee, B. H.; Kahng, Y. H.; Jo, Y.-R.; Kim, B.-J.; Lee, K. Highly Conductive PEDOT: PSS Nanofibrils Induced by Solution-Processed Crystallization. *Adv. Mater.* **2014**, *26* (14), 2268−2272.
(42) Kim, J. Y.; Jung, J. H.; Lee, D. E.; Joo, J. Enhancement of electrical conductivity of poly(3,4-ethylenedioxythiophene)/poly(4-styrenesulfonate) by a change of solvents. *Synth. Met.* **2002**, *126* (2−3), 311−316.
(43) Fabretto, M.; Hall, C.; Vaithianathan, T.; Innis, P. C.; Mazurkiewicz, J.; Wallace, G. G.; Murphy, P. The mechanism of conductivity enhancement in poly(3,4-ethylenedioxythiophene)-poly(styrenesulfonic) acid using linear-diol additives: Its effect on electrochromic performance. *Thin Solid Films* **2008**, *516* (21), 7828−7835.
(44) Stephen, M.; Wu, X.; Li, T.; Salim, T.; Hou, K.; Chen, S.; Leong, W. L. Crown ether enabled enhancement of ionic-electronic properties of PEDOT:PSS. *Mater. Horizons* **2022**, *9* (9), 2408−2415.
(45) Hossain, J.; Liu, Q.; Miura, T.; Kasahara, K.; Harada, D.; Ishikawa, R.; Ueno, K.; Shirai, H. Nafion-Modified PEDOT:PSS as a Transparent Hole-Transporting Layer for High-Performance Crystalline-Si/Organic Heterojunction Solar Cells with Improved Light Soaking Stability. *ACS Appl. Mater. Interfaces* **2016**, *8* (46), 31926−31934.

https://doi.org/10.1021/acsomega.3c09187
ACS Omega 2024, 9, 15040−15051

(46) Yu, X.; Shen, X.; Mu, X.; Zhang, J.; Sun, B.; Zeng, L.; Yang, L.; Wu, Y.; He, H.; Yang, D. High Efficiency Organic/Silicon-Nanowire Hybrid Solar Cells: Significance of Strong Inversion Layer. *Sci. Rep.* **2015**, *5*, 17371 DOI: 10.1038/srep17371.
(47) Ikeda, N.; Koganezawa, T.; Kajiya, D.; Saitow, K.-i. Performance of Si/PEDOT:PSS Hybrid Solar Cell Controlled by PEDOT:PSS Film Nanostructure. *J. Phys. Chem. C* **2016**, *120* (34), 19043−19048.
(48) Song, I.; Park, N. Y.; Jeong, G. S.; Kang, J. H.; Seo, J. H.; Choi, J.-Y. Conductive channel formation for enhanced electrical conductivity of PEDOT:PSS with high work-function. *Appl. Surf. Sci.* **2020**, *529*, No. 147176, DOI: 10.1016/j.apsusc.2020.147176.
(49) Nam, Y.-H.; Kim, D.-H.; Shinde, S. S.; Song, J.-W.; Park, M.-J.; Yu, J.-Y.; Lee, J.-H. Planar n-Si/PEDOT: PSS hybrid heterojunction solar cells utilizing functionalized carbon nanoparticles synthesized via simple pyrolysis route. *Nanotechnology* **2017**, *28* (47), 475402 DOI: 10.1088/1361-6528/aa9014.
(50) Li, Q.; Yang, J.; Chen, S.; Zou, J.; Xie, W.; Zeng, X. Highly Conductive PEDOT:PSS Transparent Hole Transporting Layer with Solvent Treatment for High Performance Silicon/Organic Hybrid Solar Cells. *Nanoscale Res. Lett.* **2017**, *12*, 506 DOI: 10.1186/s11671-017-2276-5.
(51) Srivastava, A.; Sharma, D.; Kumari, P.; Dutta, M.; Srivastava, S. K. Highly Efficient PEDOT:PSS/Silicon Hybrid Solar Cells via Effective Surface Microengineering of Low-Cost Solar-Grade Silicon Wafers. *ACS Appl. Energy Mater.* **2021**, *4* (4), 4181−4198.
(52) Han, Y.; Liu, Y.; Yuan, J.; Dong, H.; Li, Y.; Ma, W.; Lee, S.-T.; Sun, B. Naphthalene Diimide-Based n-Type Polymers: Efficient Rear Interlayers for High-Performance Silicon-Organic Heterojunction Solar Cells. *ACS Nano* **2017**, *11* (7), 7215−7222.
(53) Yameen, M.; Srivastava, S. K.; Singh, P.; Turan, K.; Prathap, P.; Vandana; Rauthan, C. M. S.; Singh, P. K. Low temperature fabrication of PEDOT:PSS/micro-textured silicon-based heterojunction solar cells. *J. Mater. Sci.* **2015**, *50* (24), 8046−8056.
(54) He, J.; Yang, Z.; Liu, P.; Wu, S.; Gao, P.; Wang, M.; Zhou, S.; Li, X.; Cao, H.; Ye, J. Enhanced Electro-Optical Properties of Nanocone/Nanopillar Dual-Structured Arrays for Ultrathin Silicon/Organic Hybrid Solar Cell Applications. *Adv. Energy Mater.* **2016**, *6* (8), 1501793 DOI: 10.1002/aenm.201501793.
(55) Fang, W.; Wang, P.; Ni, Z.; Sun, T.; Xiang, C.; Yue, K.; Wang, R.; Yang, J.; Zhou, Y.; Wang, C.; Yang, Y. Planar Organic-Si Hybrid Solar Cell with MoO_x Mixed PEDOT:PSS as Hole Injection Layer Profits from Mo^{5+} and Mo^{6+} Synergistic Effects. *Adv. Mater. Interfaces* **2020**, *7* (19), 2000754 DOI: 10.1002/admi.202000754.
(56) Richter, A.; Müller, R.; Benick, J.; Feldmann, F.; Steinhauser, B.; Reichel, C.; Fell, A.; Bivour, M.; Hermle, M.; Glunz, S. W. Design rules for high-efficiency both-sides-contacted silicon solar cells with balanced charge carrier transport and recombination losses. *Nat. Energy* **2021**, *6*, 429 DOI: 10.1038/s41560-021-00805-w.

https://doi.org/10.1021/acsomega.3c09187
ACS Omega 2024, 9, 15040−15051